5648 *Inorg. Chem.* **2009**, *48*, 5648–5662
DOI: 10.1021/ic801294x

Inorganic Chemistry
Article

Microcrystalline Hexagonal Tungsten Bronze. 1. Basis of Ion Exchange Selectivity for Cesium and Strontium

Christopher S. Griffith,*,† Vittorio Luca,*,†,§ John V. Hanna,†,# Kevin J. Pike,‡ Mark E. Smith,‡ and Gordon S. Thorogood†

†*Australian Nuclear Science and Technology Organisation, ANSTO Minerals, New Illawarra Road, Lucas Heights, NSW 2234, Australia, and* ‡*Department of Physics, University of Warwick, Gibbet Hill Rd., Coventry CV4 7AL, United Kingdom.* §*Present address: Comisión Nacional de Energía Atómica, Centro Atómico Constituyentes, Av. General Paz 1499,1650 San Martin, Provincia de Buenos Aires, Argentina.* #*Present address: Department of Physics, University of Warwick, Gibbet Hill Rd., Coventry CV4 7AL, United Kingdom.*

Received July 10, 2008

The structural basis of selectivity for cesium and strontium of microcrystalline hexagonal tungsten bronze (HTB) phase $Na_xWO_{3+x/2}\cdot zH_2O$ has been studied using X-ray and neutron diffraction techniques, 1D and 2D ^{23}Na magic angle spinning (MAS) nuclear magnetic resonance (NMR) spectroscopy, and radiochemical ion exchange investigations. For the HTB system, this study has shown that scattering techniques alone provide an incomplete description of the disorder and rapid exchange of water (with tunnel cations) occurring in this system. However, 1D and 2D ^{23}Na MAS NMR has identified three sodium species within the HTB tunnels—species A, which is located at the center of the hexagonal window and is devoid of coordinated water, and species B and C, which are the di- and monohydrated variants, respectively, of species A. Although species B accords with the traditional crystallographic model of the HTB phase, this work is the first to propose and identify the anhydrous species A and monohydrate species C. The population (total) of species B and C decreases in comparison to that of species A with increasing exchange of either cesium or strontium; that is, species B and C appear more exchangeable than species A. Moreover, a significant proportion of tunnel water is redistributed by these cations. Multiple ion exchange investigations with radiotracers ^{137}Cs and ^{85}Sr have shown that for strontium there is a definite advantage in ensuring that any easily exchanged sodium is removed from the HTB tunnels prior to exchange. The decrease in selectivity (wrt cesium) is most probably due to the slightly smaller effective size of Sr^{2+}; namely, it is less of a good fit for the hexagonal window, ion exchange site. The selectivity of the HTB framework for cesium has been shown unequivocally to be defined by the structure of the hexagonal window, ion exchange site. Compromising the geometry of this window even in the slightest way by either (1) varying the cell volume through changes to hydration or sodium content or (2) introducing disorder in the $a-b$ plane through isomorphous substitution of molybdenum is sufficient to reduce the selectivity. Indeed, it is our hypothesis that this applies for all cations which are strongly bound by the HTB framework.

1. Introduction

Highly acidic aqueous solutions containing the entire gamut of fission products and minor actinides can result from a range of nuclear activities including irradiated fuel reprocessing and medical isotope production. Radiogenic cesium and strontium comprise a majority of the activity after about 4−5 years and are also two of the most prolific heat-generating isotopes, whereas long-term radiotoxicity is primarily a product of the long-lived minor actinides. The selective extraction of these high heat-load elements can greatly simplify downstream processing and aid in the overall volume reduction of these wastes with the consequence that precious repository space is conserved.[1] Because of the high radioactivity of such waste solutions, inorganic ion exchangers have generally been considered more preferable to organic resins. The past several decades have therefore seen a significant effort aimed at developing or discovering new ion exchange materials for such applications.

Zeolites are the archetypal inorganic ion exchangers, and it is their tunnel architectures that are at least in part responsible for the very high selectivity they display for different elements. The natural zeolite, clinoptilolite, is the most abundant of the natural zeolites and has attracted considerable attention for the removal of heavy metals from

*To whom correspondence should be addressed. Tel: 54-11-6772 7018. E-mail: vluca@cnea.gov.ar (V.L.), christopher.griffith@ansto.gov.au (C.S.G.).

(1) Todd, T. A.; Brewer, K. N.; Law, J. D.; Wood, D. J.; Garn, T. G.; Tillotson, R. D.; Tullock, P. A.; Wade, E. L. *Waste Manage.* **1997**, 2368.

Published on Web 06/11/2009

a variety of aqueous solutions including mine wastes,[2] milk,[3] and drinking water.[4] Clinoptilolite has also attracted considerable interest in the radioactive waste management context, owing to its excellent selectivity for cationic species such as Cs^+.[5−9] While clinoptilolite can easily extract small concentrations of Cs^+ from solutions having a high background concentration of other cations, and although its stability to ionizing radiation is good,[10] its hydrolytic stability is limited,[11] and therefore it is probably better suited to groundwater treatment rather than to treatment of acidic radioactive waste streams. Such limitations have helped prompt an extensive international search for more stable yet highly Cs- and Sr-selective materials. A new material that was derived from this effort was the mixed framework zeolite-like titanosilicate known as sitinakite, which can extract parts per million concentrations of Cs^+ from highly caustic and acidic radioactive solutions that are in excess of 4 M in sodium.[12−15] Other potentially useful inorganic ion exchangers include the polyoxomolybdates[16,17] and hexacyanoferrates,[18,19] although again, the former has limited stability in acidic solution.[20] Despite all of this activity, the basis of the selectivity of all but a few are well-understood. One inorganic system that has been intensively studied, and the selectivity of which is consequently well-understood, is the synthetic analogue of the previously mention mineral known as sitinakite.[21] Clearly, however, as in the case of extractant molecules such as the cyclic polyethers and biological membranes (see Laio and Torre[22] and references therein), it is the fit of the target species within the cavity or tunnel that seems to be a major factor in defining the adsorption/extraction properties of inorganic ion exchangers also.

An additional consideration in deploying an inorganic ion exchange material in a nuclear waste management application is the need to consider the fate of the spent or saturated ion exchanger, as this tends to narrow the range of useful materials. One option is to combine the spent ion exchanger with other components and melt the mixture to form a waste glass or ceramic material suitable for repository emplacement. Another option is to convert the material directly into a durable waste form via simple thermal processing. In regard to the latter more elegant and simpler approach, it has been demonstrated that the aforementioned silico-titanate materials can indeed be thermally converted to durable materials, and the nature of this conversion process has been studied in detail.[23−27]

Recently, we discovered that hydrous tungsten oxides with the hexagonal tungsten bronze (HTB) structure, which are highly stable in acidic solution, also display high selectivity for Cs^+ and Sr^{2+}. The first HTB-like phase, $WO_3 \cdot {}^1/_3H_2O$, was synthesized using the wet chemical methods reported by Gerand and co-workers.[28] The synthesis of the first HTB phase containing exchangeable cations in tunnel sites was reported by Reis and co-workers through adjustment of the pH of a sodium tungstate solution followed by hydrothermal treatment at low temperatures (140−200 °C).[29−32] We have already reported on the isomorphous substitution of molybdenum for tungsten in this system and the effect that this has on the observed ion exchange properties using micromolar concentrations in acidic solutions.[33] The structure of the HTB phase with nominal formula $Na_xWO_{3+x/2} \cdot zH_2O$ (Na−W−HTB) has been analyzed using neutron diffraction and Rietveld refinement.[29] The structure was refined in the space group $P6/mmm$ and was reported to be similar to that of high-temperature reduced HTB except that it contained Na^+ ions at the (0, 0, 0) position (Figure 1a). Commonly, this position is referred to as being at the center of the "hexagonal window", which is easily visualized using the additional projections shown in Figure 1b and c. Along with cations in the hexagonal tunnel architecture, water molecules were also present with the water oxygen positioned at (0, 0, ∼0.4). In addition to water molecules, oxygen anions and hydroxyl groups of the framework may also be present in these tunnel positions, but to our knowledge, these species have never been located using structural techniques. The tunnel dimensions of these materials are much more restrictive than observed in most microporous zeolites and all of the silico-titanates, which might be expected to make transport through the tunnel architecture more constrained and also more susceptible to small changes in lattice dimensions induced by isomorphic substitutions into the lattice as well

(2) Zamzow, M. J.; Murphy, J. E. *Sep. Sci. Technol.* **1992**, *27*, 1969.
(3) De Villiers, W. V. Z.; De Klerk, S. *Radiochim. Acta* **1991**, *54*, 205.
(4) Blanchard, G.; Maunaye, M.; Martin, G. *Water Res.* **1984**, *18*, 1501.
(5) Behrens, E. A.; Sylvester, P.; Clearfield, A. *Environ. Sci. Technol.* **1998**, *32*, 101.
(6) Faghihian, H.; Marageh, M. G.; Kazemian, H. *Appl. Radiat. Isot.* **1999**, *50*, 655.
(7) Howden, M.; Pilot, J. *Ion Exch. Technol.* **1984**, 66.
(8) Rhodes, D. W.; Wilding, M. W. *U.S. At. Energy Comm.* **1965**, *IDO-14657*, 16.
(9) Elizondo, N. V.; Ballesteros, E.; Kharisov, B. I. *Appl. Radiat. Isot.* **2000**, *52*, 27.
(10) Moraetis, D.; Christidis, G. E.; Perdikatsis, V. *Am. Mineral.* **2007**, *92*, 1714.
(11) Murphy, W. M.; Pabalan, R. T.; Prikryl, J. D.; Goulet, C. J. *Am. J. Sci.* **1996**, *296*, 128.
(12) Latheef, I. M.; Huckman, M. E.; Anthony, R. G. *Ind. Eng. Chem. Res.* **2000**, *39*, 1356.
(13) Zheng, Z.; Anthony, R. G.; Miller, J. E. *Ind. Eng. Chem. Res.* **1997**, *36*, 2427.
(14) Zheng, Z.; Gu, D.; Anthony, R. G.; Klavetter, E. *Ind. Eng. Chem. Res.* **1995**, *34*, 2142.
(15) Anthony, R. G.; Philip, C. V.; Dosch, R. G. *Waste Manage.* **1993**, *13*, 503.
(16) Tranter, T. J.; Herbst, R. S.; Todd, T. A.; Olson, A. L.; Eldredge, H. B. *Adv. Environ. Res.* **2002**, *6*, 107.
(17) Todd, T. A.; Mann, N. R.; Tranter, T. J.; Sebesta, F.; John, J.; Motl, A. *J. Radioanal. Nucl. Chem.* **2002**, *254*, 47.
(18) Lehto, J.; Harjula, R. *Solvent Extr. Ion Exch.* **1987**, *5*, 343.
(19) Lehto, J.; Paajanen, A.; Harjula, R. *J. Radioanal. Nucl. Chem.* **1992**, *164*, 39.
(20) Miller, C. J.; Olson, A. L.; Johnson, C. K. *Sep. Sci. Technol.* **1997**, *32*, 37.
(21) Celestian, A. J.; Kubicki, J. D.; Hanson, J.; Clearfield, A.; Parise, J. B. *J. Am. Chem. Soc.* **2008**, *130*, 11689.
(22) Laio, A.; Torre, V. *Biophys. J.* **1999**, *76*, 129.
(23) Balmer, M. L.; Su, Y.; Nenoff, T. M.; Navrotsky, A.; Bunker, B. C. *Book of Abstracts*, 215th ACS National Meeting, Dallas, March 29−April 2, **1998**; American Chemical Society: Washington, DC; p I&EC-090.
(24) Nyman, M.; Nenoff, T. M.; Su, Y.; Balmer, M. L.; Navrotsky, A.; Xu, H. *Mater. Res. Soc. Symp. Proc.* **1999**, *556*, 71.
(25) Su, Y.; Balmer, M. L.; Wang, L.; Bunker, B. C.; Nyman, M.; Nenoff, T.; Navrotsky, A. *Mater. Res. Soc. Symp. Proc.* **1999**, *556*, 77.
(26) Su, Y.; Balmer, M. L.; Bunker, B. C. *Mater. Res. Soc. Symp. Proc.* **1997**, *465*, 457.
(27) Nyman, M.; Gu, B. X.; Wang, L. M.; Ewing, R. C.; Nenoff, T. M. *Microporous Mesoporous Mater.* **2000**, *40*, 115.
(28) Gerand, B.; Nowogrocki, G.; Guenot, J.; Figlarz, M. *J. Solid State Chem.* **1979**, *29*, 429.
(29) Reis, K. P.; Prince, E.; Whittingham, M. S. *Chem. Mater.* **1992**, *4*, 307.
(30) Reis, K. P.; Ramanan, A.; Whittingham, M. S. *Chem. Mater.* **1990**, *2*, 219.
(31) Reis, K. P.; Ramanan, A.; Whittingham, M. S. *J. Solid State Chem.* **1992**, *96*, 31.
(32) Reis, K. P.; Ramanan, A.; Gloffke, W.; Whittingham, M. S. *Mater. Res. Soc. Symp. Proc.* **1991**, *210*, 473.
(33) Griffith, C. S.; Luca, V. *Chem. Mater.* **2004**, *16*, 4992.

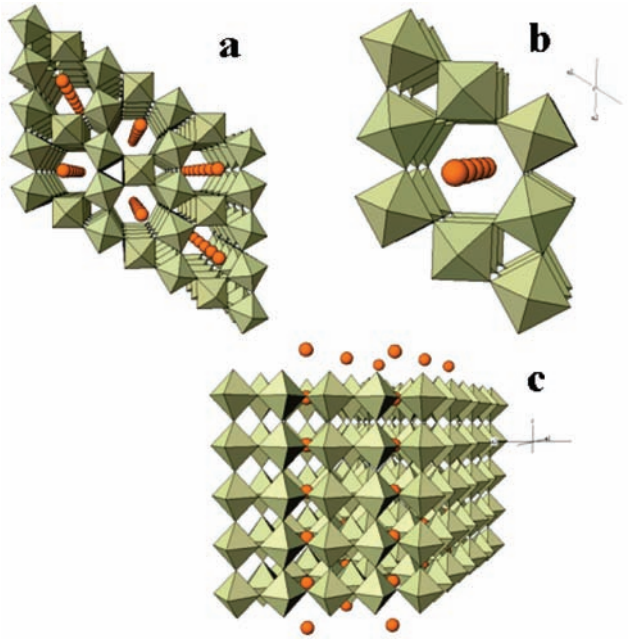

Figure 1. (a) Projection of HTB framework as viewed down the *c*-axis. (b) Selective projection of HTB framework as viewed down the *c*-axis. (c) Projection of HTB framework as viewed on the *a*−*c* plane, approximately 30° from the *b* axis. Sodium occupancies at the *1a* (0, 0, 0) position are set equal to 1 in each projection.

as the level of hydration. Indeed, we have shown in previous published work that relatively low-temperature heating can essentially lock in these exchangeable cations.[34−38]

For the low-temperature, hydrothermally synthesized Na−W−HTB phase, it has long been known that a proportion of the tunnel Na^+ atoms are relatively easily replaced by other alkali metal atoms including K^+, Cs^+, alkaline earth cations, and trivalent cations.[30] What is not generally appreciated is the fact that the tunnel dimensions appear to impart a particularly high selectivity for cations with ionic radii around 1.2 and 1.7 Å and this makes HTB materials quite selective for Cs^+ and Sr^{2+} in acidic media and, therefore, potentially useful for the pretreatment of radioactive wastes.

The aim of the present contribution is to elucidate the nature of the Na^+, Cs^+, and Sr^{2+} cation siting in these materials and then link this to the ion exchange behavior/mechanism of the microporous hexagonal tungsten bronze phase $Na_xWO_{3+x/2}.zH_2O$, using X-ray and neutron diffraction techniques, 1D and 2D ^{23}Na magic angle spinning (MAS) nuclear magnetic resonance (NMR) spectroscopy, and radiochemical ion exchange investigations. The effect on selectivity/affinity when isomorphous substitution of molybdenum for tungsten occurs has also been readdressed.

2. Experimental Section

2.1. General. Standard laboratory-grade reagents (>98% purity) from Sigma Aldrich were employed for all syntheses and ion exchange investigations. Elemental analysis of materials was undertaken by both energy dispersive spectroscopy (EDS), which was coupled to a JEOL 6400m scanning electron microscope, and X-ray florescence (XRF) analysis. XRF measurements were conducted using a wavelength dispersive Philips PW2400 X-ray Fluorescence Spectrometer equipped with a rhodium anode tube. Samples were prepared by pressing in boric acid and the results analyzed using the Uniquant software suite. Thermogravimetric (TG) and differential thermal (DT) analyses were conducted simultaneously on a Setaram TAG24 (France) with high-purity air carrier gas. Bulk particle size distributions were measured using a Malvern Mastersizer 2000 (Malvern Pty Ltd., England). Samples were dispersed in water, stirred (2 min), then subjected to ultrasonication (initial, 2 min; final, 4 min) before measurement.

2.2. Synthesis of $Na_{0.2}Mo_yW_{1-y}O_3\cdot zH_20$ (y = 0−0.2). The hexagonal tungsten bronze (Na−W−HTB, y = 0) phase was prepared according to the methodology of Reis and co-workers,[30,31] in which Na_2WO_4 solution (1 M) was acidified with HCl (1 M) to within the pH range 1.65−1.75. Hydrothermal treatment (155 °C, 30−48 h) of the resultant solution was undertaken in Teflon-lined Parr acid digestion bombs to afford a pale green solid, which was collected by filtration and washed with 1 M HNO_3 and then deionized water until the pH of the filtrate was neutral. The solid was dried to a constant weight at 75 °C in the air and stored in the absence of light. The preparation of variably molybdenum-doped phases (Na−Mo_y−HTB; y = attempted Mo atom % substitution level) was undertaken by adding the required quantity of Na_2MoO_4 solution (1 M) to the Na_2WO_4 solution prior to acidification and hydrothermal treatment.

2.3. Synthesis of $A_xWO_3\cdot zH_20$ (A = H, Cs, Sr). Variably Cs- or Sr-exchanged W−HTB samples were prepared by contacting the parent $Na_{0.2}WO_3\cdot zH_2O$ (Na−W−HTB; ∼2 g) with acidic solutions (50 mL, 1 M HNO_3) containing an increasing concentration of the given metal cation for 24 h. During this time, the reaction mixtures were agitated then filtered and the resultant solid washed with deionized water until the pH of the filtrate was neutral. The solids were dried to a constant weight at 75 °C in the air and stored in the absence of light. The uptake of either Cs^+ or Sr^{2+} (mmol g^{-1}) was calculated on the basis of the initial and final concentrations in solution, as determined by ICPMS and the initial weight of Na−W−HTB.

Samples of Na−W−HTB where variable levels of Na^+ were present were prepared by contact (24 h) with either 1, 3, 6, 9, or 15 M HNO_3. The solids were then filtered and the resultant solid washed with deionized water until the pH of the filtrate was neutral. The solids were dried to a constant weight at 75 °C in air and stored in the absence of light. The level of sodium remaining after acid treatment was initially determined using EDS and confirmed by routine XRF analysis.

2.4. Ion Exchange Behavior−Radiochemical Analysis. The ion exchange behaviors of variably exchanged W−HTB materials were investigated in triplicate using the batch contact method. For carrier-free investigations, powdered sorbent (50 ± 1 mg) and a given nitric acid concentration solution (0.1−9 M; 4 mL) containing approximately 1×10^{-6} cpm of ^{137}Cs (>99% purity; I^3 Inc., Idaho Falls) or ^{85}Sr (>98% purity; Perkin-Elmer, USA) were contacted at 25 °C for 30 min with agitation in a glass Kimble tube (5 mL). The appropriateness of the contact time was ascertained by performing a series of experiments with each radioisotope where the contact time was varied from 5 to 60 min. The effect of the inactive carrier was determined by the addition of a concentrated solution (1 M) of the appropriate cation so as to achieve a final concentration of approximately 2 ppm with respect to the carrier cation. After the required contact time, the reaction mixtures were centrifuged (5000 rpm, 7 min) and three separate 1 mL aliquots of each supernatant removed for analysis. Triplicate samples of the

(34) Luca, V.; Griffith, C. S.; Chronis, H.; Widjaja, J.; Scales, N. *Mater. Res. Soc. Symp. Proc.* **2004**, *807*, 309.
(35) Luca, V.; Drabarek, E.; Griffith, C. S.; Chronis, H.; Foy, J. *Mater. Res. Soc. Symp. Proc.* **2004**, *807*, 303.
(36) Luca, V.; Griffith, C. S.; Drabarek, E.; Chronis, H. *J. Nucl. Mater.* **2006**, *358*, 139.
(37) Griffith, C. S.; Šebesta, F.; Hanna, J. V.; Yee, P.; Drabarek, E.; Smith, M. E.; Luca, V. *J. Nucl. Mater.* **2006**, *358*, 151.
(38) Luca, V.; Drabarek, E.; Chronis, H.; Mcleod, T. *J. Nucl. Mater.* **2006**, *358*, 164.

initial ^{137}Cs or ^{85}Sr activities and triplicate samples of the individual contact experiments were counted for 10−20 s on an automated Wallac 1480 Wizard 3″ γ counter using the 661 and 514 keV γ emissions, respectively. Decay corrections were applied during counting. The activities of the initial solutions and final supernatants were taken as the average of the triplicate analyses and the respective errors calculated using the range of the three analyses.

Determination of the given radioisotope activities before and after contact with a given sorbent allows the calculation of a distribution coefficient (K_d) for the given radioisotope with respect to the sorbent using the formula

$$K_d = \frac{A_i - A_f}{A_f} \cdot \frac{V}{m} \cdot F$$

where A_i = initial cation concentration, A_f = final cation concentration, V = volume of the solution contacted with the sorbent, m = mass of the sorbent employed, and F = form factor (%) to normalize for hydration of the given sorbent. All batch contact experiments were conducted using $V/m \cong 80$ mL g^{-1} in order to allow a direct comparison of results.

2.5. X-Ray Diffraction. Survey powder X-ray diffraction patterns of the Na−W−HTB, variably Cs- and Sr-exchanged W−HTB, and Mo_y−HTB phases were recorded on a Panalytical X'Pert Pro diffractometer in the range 5−80° 2θ using Cu Kα radiation (1.542 Å) and employing a solid-state detector utilizing real-time multiple strip technology. Rietveld modeling was performed using the Rietica-LHPM software,[39] which derives from the Hill−Howard−Hunter LHPM program.[40]

2.6. Neutron Diffraction. Powder neutron diffraction data were collected on the medium-resolution powder Diffractometer (λ = 1.6649 Å) at the HIFAR facility of the Australian Nuclear Science and Technology Organisation. The A−W−HTB (A = Na, Cs, Sr) phases were first dried under vacuum at 373 K for 72 h in an attempt to remove the majority of H_2O without altering the tungstate framework. After cooling, the samples were contacted with degassed D_2O under an atmosphere of dry nitrogen for 24 h. The supernatant was then removed and samples dried under vacuum conditions (∼2 mTorr) at ambient temperature. Loading of samples into vanadium cans (Viton O-ring seal) was conducted in a dry (< 1 ppm H_2O), argon-filled glovebox. Data were acquired at ambient temperature (303 K) over an angular range of 6−132° in increments of 0.1°. Refinements of the data were conducted using the Reitica software package.[39]

2.7. Solid-State ^{23}Na MAS NMR. High-resolution ^{23}Na MAS NMR data were acquired at ambient temperatures on a Bruker MSL-400 spectrometer (B_0 = 9.4 T) operating at the ^{23}Na frequency of 105.81 MHz. All 1D data were acquired using single-pulse (Bloch decay) experiments with a Bruker 4 mm double-air-bearing probe from which typical MAS frequencies of ∼15 kHz were implemented. For the ^{23}Na MAS NMR measurements, nonselective $\pi/2$ pulse times of 3.0 μs were measured on a 1.0 M NaCl solution, from which selective pulse times of ∼0.6 μs were employed for data acquisition on all solid samples. Recycle delays of 3 s were typically used; however, the quantification and speciation of these data obtained with shorter recycle delays were verified with experiments which had delays extending to 30 s. All ^{23}Na chemical shifts were referenced to 1.0 M NaCl, which was set to δ 0.0 ppm. All ^{23}Na shifts (δ) are reported as center-of-gravity measurements and remain uncorrected for second-order quadrupolar effects unless specifically reported as isotropic values (δ_{iso}) obtained from simulation or graphical methods.

^{23}Na two-dimensional multiple-quantum magic-angle-spinning (2D MQ-MAS) NMR studies[41−44] were undertaken at magnetic field strengths of B_0 = 8.45 and 14.1 T using Varian/Chemagnetics Infinity-360 and Infinity-600 spectrometers, respectively. At B_0 = 8.45 T (95.25 MHz), an amplitude-modulated triple-quantum (3Q) MAS NMR experiment[41,45] was used which provided high-resolution hyper-complex 2D spectra whose indirectly detected (F_1) dimensions have sign discrimination and are free from the second-order quadrupolar broadening exhibited by the central transition of the spin I = 3/2 ^{23}Na isotope. These measurements were achieved using a Bruker 4 mm probe and MAS rates of ∼8−10 kHz. In these experiments, 5.5 μs 3Q excitation pulses and 2.5 μs 3Q conversion pulses were utilized with RF field strengths of B_1 = 110 kHz, in conjunction with reduced power (B_1 = 16 kHz) Z-filter pulses of 9 μs duration. Typical relaxation delays were 1 s, and each experiment took approximately 24 h. At 14.1 T (158.83 MHz), a phase-modulated split-t1 3Q MAS sequence[41] was implemented using a Varian 3.2 mm T3 probe and MAS rates of ∼10 kHz. For these experiments, 3.2 μs excitation pulses (B_1 = 155 kHz) and 10.0 μs echo pulses (B_1 = 30 kHz) were used. Maximum-strength (B_1 = 155 kHz) single-period, sine-modulated 3Q conversion pulses of 4.0 μs periods were used to reduce the intensity lost by large C_Q lineshapes in the 3Q MQ-MAS NMR data. The echo times were 1.2 ms, relaxation delays were 2 s, and each experiment took approximately 24 h.

A variable B_0 field study of the ^{23}Na resonances characterizing these systems was also undertaken. To effect this study, additional 1D MAS data were acquired at the external B_0 field strengths of 7.05, 8.45, and 14.1 T. Similar pulse and recycle delay conditions were implemented as described above, with accurate chemical shift referencing against 1.0 M NaCl (δ 0.0 ppm) being maintained throughout. All ^{23}Na MAS data were simulated using the dmfit NMR data fitting program[46] with the apparent shift positions gained from this deconvolution at each B_0 field used to determine the representative δ_{iso} and P_Q spectral parameters for each site from established quantum mechanical principles and

(39) Hunter, B. A. *International Union of Crystallography, Commission on Powder Diffraction Newsletter* **1998**, *20*, 21.
(40) Hill, R. J.; Howard, C. J.; Hunter B. A. *Computer Program for Rietveld Analysis of Fixed Wavelength X-Ray and Neutron Powder Diffraction Patterns, Australian Atomic Energy Commission (Now ANSTO). Rept. No. M112*, Lucas Heights Research Laboratories, New South Wales, Australia, **1995**.
(41) Brown, S. P.; Wimperis, S. *J. Magn. Reson.* **1997**, *128*, 42.
(42) Fernandez, C.; Amoureux, J. P. *Chem. Phys. Lett.* **1995**, *242*, 449.
(43) Medek, A.; Harwood, J. S.; Frydman, L. *J. Am. Chem. Soc.* **1995**, 12779.
(44) Frydman, L.; Harwood, J. S. *J. Am. Chem. Soc.* **1995**, *117*, 5367.
(45) Amoureux, J.-P.; Fernandez, C.; Steuernagel, S. *J. Magn. Reson.* **1996**, *123*, 116.
(46) Massiot, D.; Fayon, F.; Capron, M.; King, I.; Le Calvé, S.; Alonso, B.; Durand, J.-O.; Bujoli, B.; Gan, Z.; Hoatson, G. *Magn. Reson. Chem.* **2002**, *40*, 70.

graphical methods.[47−52] In more difficult cases arising for the parent Na−W−HTB phase, where large distributions and unresolved line width issues prohibited an effective variable B_0 analysis, a reduced B_0 field approach using the 2D MQ-MAS data was implemented. In this case, the simulated positions were supplemented by those obtained using the 2D maxima (F_2 or MAS dimension) and the vertical projections (F_1 or isotropic dimension) from the MQ-MAS data acquired at 8.45 and 14.1 T. The scaling of the apparent shifts in these data causes these points to occur on opposite sides of the origin.[50]

Samples for NMR analysis were dehydrated at various temperatures in a conventional laboratory oven and were transferred directly from the oven to a nitrogen-filled glovebox in which the H_2O and O_2 contents were <1 ppm. Within these glovebox conditions, all samples were transferred into sealed polyethylene bottles. These bottles were stored under these anhydrous conditions until the subsequent transferal of each sample into airtight NMR rotors was performed, which was similarly undertaken under these controlled glovebox conditions.

3. Results and Discussion

3.1. Structure of Hexagonal Tungsten Bronzes ($A_xWO_3 \cdot zH_2O$, A = Na, x = 0.2; A = Cs, x = 0.16; A = Sr, x = 0.08)—Neutron Diffraction. Refinements of the neutron powder diffraction data for the parent hydrated Na-, Sr-, and Cs-exchanged phases were performed using the reported structural model[29] of the hydrated hexagonal tungsten bronze as a starting point. The neutron diffraction data and associated refinements and residual plots are shown in the Supporting Information section. The space group chosen was *P6/mmm*, with the atoms placed at the following positions: W, *3f* site (0.5, 0, 0); O(1), *3g* (0.5, 0, 0.5); O(2), *6l* (x, 2x, 0), where x = 0.21; Na, *1a* (0, 0, 0); and O(3), 2e (0, 0, 0.412). During these refinements, it was clearly evident that the *1a* (0, 0, 0) site of the tunnel cations was not fully occupied in any of the three phases studied. The thermal parameters of both Sr and Na had to be set at 1.0 and 2.0 to obtain even a satisfactory refinement of the tungstate framework. However, the goodness of fit parameters were reasonable in light of the fact that a large amount of H_2O had not been exchanged for D_2O despite attempts to the contrary (see the Experimental Section). The refinements of each data set clearly indicated significant positional disorder of the tunnel cations and H and D atoms of the tunnel water molecules. Importantly, there was no evidence to suggest that the *1a* (0, 0, 0) position was not the correct assignment from these data. The refinement of the neutron data for the Na− and Cs−W−HTB phases unequivocally demonstrated that the tunnel cations all lie at the center of the hexagonal window in the W_6O_6 plane, as the location of the tunnel cation in anything other than the *1a* (0, 0, 0) position afforded refinements which were unstable or significantly inferior to that obtained using the *1a* assignment, in much the same way as that reported by Reis et al.[29] In the case of the Sr−W−HTB phase, the Sr^{2+} cation experienced significant disorder, so much so that very little regular scattering by Sr was observed. This was evident from a dramatic decrease in the intensity of the [010] reflection (see the Supporting Information for refinement plots). The inability to locate the cations more precisely makes the establishment of direct structure−function relationships difficult on the basis of scattering data alone, as these techniques only provide an averaged picture of the structure. However, it would appear that the exchange of Cs or Sr into the tungstate framework increases the mobility of the species within the tunnels, leading to increased positional disorder of the cations.

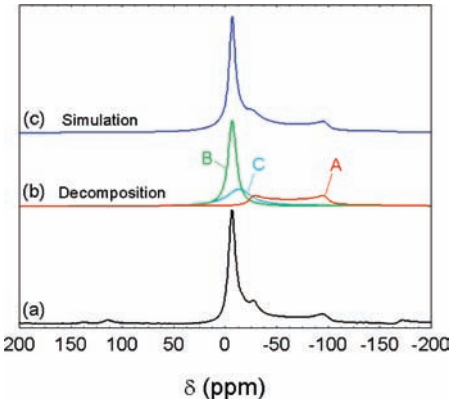

Figure 2. ^{23}Na MAS NMR spectra acquired at 9.4 T of parent Na−W−HTB (a) along with the individual components (b) and spectral simulation (c).

3.2. Solid State 1D and 2D ^{23}Na MAS NMR. Solid-state NMR techniques are particularly well-placed to provide a detailed, localized perspective of an exchangeable cation siting in hydrous oxide materials with tunnel architectures, as the technique is inherently sensitive to the immediate coordination sphere about the nucleus of interest. In the present study and the following companion article in this journal (part 2), the higher gyromagnetic ratios and lower quadrupole moments of nuclei such as ^{23}Na (I = $^3/_2$) and ^{133}Cs (I = $^7/_2$) (γ = 7.0809 × 10^7 rad s^{-1} T^{-1}/Q = 10.4 fm^2 and γ = 3.5333 × 10^7 rad s^{-1} T^{-1}/Q = −0.34 fm^2, respectively) coupled with the 100% abundance of these isotopes has enabled a probe of local speciation to be undertaken with great sensitivity. This contrasts with the low γ/high Q ^{87}Sr (I = $^9/_2$) nucleus (γ = −1.16394 × 10^7 rad s^{-1} T^{-1}/Q = 33.5 fm^2), which also possesses a low natural abundance of ∼7%, thus rendering it effectively observable at high B_0 fields (B_0 > 16.4 T) only, and in situations where some short-range order exists.

The ^{23}Na MAS NMR spectra of parent Na−W−HTB are shown in Figure 2a together with the spectral deconvolution (Figure 2b) and the total simulation (Figure 2c) in order to demonstrate the influence that hydration has on the observable Na tunnel speciation. The ^{23}Na MAS data for the parent Na−W−HTB exhibit two primary features: a very broad quadrupolar-dominated resonance spanning a width of ∼150 ppm (species A) and narrower featureless resonance(s) with a center of gravity located at

(47) Samoson, A. *Chem. Phys. Lett.* **1985**, *119*, 29.
(48) Jager, C. *NMR Basic Principles and Progress*; Springer-Verlag: Berlin, **1994**; Vol. *31*, p 135.
(49) Millot, Y.; Man, P. P. *Solid State Nucl. Magn. Reson.* **2002**, *21*, 21.
(50) Anupold, T.; Reinhold, A.; Sarv, P.; Samoson, A. *Solid State Nucl. Magn. Reson.* **1998**, *13*, 87.
(51) MacKenzie, K. J. D.; Smith, M. E. *Multinuclear Solid State NMR of Inorganic Materials*; Pergamon Press: Oxford, **2002**.
(52) Samoson, A. *J. Magn Reson. A* **1996**, *121*, 209.

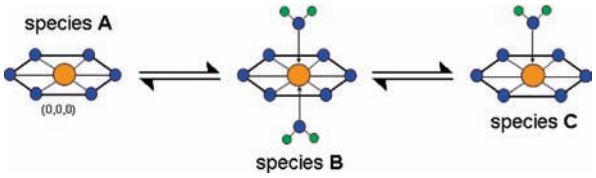

Figure 3. Schematic representation of tunnel sodium speciation for the Na−W−HTB phase based on the ^{23}Na NMR studies. Large orange spheres in the centers of the hexagons are sodium atoms, blue spheres are oxygen atoms, and smaller green spheres are hydrogen atoms belonging to water molecules.

about δ −6 to −15 ppm. The simulation and deconvolution of these data for the parent Na−W−HTB shown in Figure 2 reveal a Na tunnel species (species A) characterized by a very large quadrupolar constant (C_Q) of 5.2 MHz at an isotropic chemical shift (δ_{iso}) of −4.0 ppm. This Na site is consistent with the expected crystallographic hexagonal tunnel window position at (0, 0, 0) and represents a hexagonal planar site with short Na−O distances. The high point symmetry of this position (a C_6 axis of rotation) demands that the asymmetry parameter (η) be 0. Very large C_Q values for this type of hexagonal planar site symmetry have been predicted by Koller et al. using point charge calculation methods.[53] From these simplistic calculations, C_Q values on the order of ∼5−7 MHz are predicted for square-planar and hexagonal planar sites and are in general agreement with this assignment and the calculated C_Q value for the Na−W−HTB system. A C_Q value of 5.2 MHz is among the largest to be measured for any ^{23}Na system and is surpassed only by values of 11.34 MHz for Na_3OCl,[54] 5.90 MHz for the near-hexagonal planar tunnel site in the sodalite $Na_6[AlSiO_4]_6$,[55,56] and 5.80 MHz for the hexagonal planar tunnel site in the dehydrated zeolite NaA.[57] For an axially symmetric Na tunnel position to exhibit an electric field gradient of this magnitude in the Na−W−HTB phase, this site must assume a completely anhydrous state within its primary coordination sphere; that is, there exists discrete hexagonal planar oxo-coordination to the Na^+ cations within the tunnel confines only. The data of Figure 2 also show two additional narrower ^{23}Na resonances with apparent shifts of δ −6 ppm and δ −14 ppm that require consideration. Given the much reduced linewidths (and P_Q's) in comparison to the large C_Q site (species A), these resonances appeared likely to be hydrated variants of this site, in accord with the crystallographic model. Further, more definitive assignments can be attempted with these δ −6 ppm and δ −14 ppm resonances being due to dihydrated and monohydrated species (species B and C, respectively) based on the magnitude of the chemical shift difference from purely hydrated Na^+. The three identified tunnel sodium species (A, B, and C) are schematically represented in Figure 3. In part 2 of this study, we discuss in depth the ^{23}Na solid-state NMR of this class of materials and provide evidence in support of these assignments.

More precise information characterizing these hydrated moieties was elucidated from an analysis of the variable B_0 field behavior of these resonances. From well-established quantum mechanical treatments of the MAS NMR properties of quadrupolar nuclei, at any particular B_0 field, the apparent shift or center of gravity of a central ($-1/2 \leftrightarrow +1/2$) transition resonance is given by the sum

$$\delta_{cg} = \delta_{iso} + \delta^{(2)}_{Q,iso}(I,m)$$

where the isotropic shift δ_{iso} is augmented by a field- and spin-number-dependent second-order quadrupolar shift term $\delta^{(2)}_{Q,iso}(I,m)$ which can be expressed as[47,48]

$$\delta_{cg} = \delta_{iso} + \delta^{(2)}_{Q,iso}(I,m)$$

$$= [3C_Q^2/(40\nu_0^2 I^2(2I-1)^2)][I(I+1)$$

$$-9m(m-1)-3](1+\eta^2/3)$$

Hence, if the variation in δ_{cg} is monitored as a function of B_0 (i.e., with δ_{cg} being plotted against $1/\nu_0^2$), then by graphical methods the isotropic shift δ_{iso} and the quadrupolar interaction constant P_Q are obtained from the y intercept and slope of these data, respectively. The quadrupolar interaction constant P_Q is given by[49,50,52]

$$P_Q = C_Q\sqrt{(1+\eta^2/3)}$$

where the quadrupole coupling constant C_Q and its asymmetry parameter η are degenerate within this expression. From the variable B_0 data for Na−W−HTB presented in Figure 4a, sufficiently resolved and undistorted data could only be identified for species C at 14.1, 9.4, and 8.45 T. A graphical solution to these data yielded δ_{iso} and P_Q values of −19.4 ppm and 0.84 MHz (see Table 1), respectively; however, due to the inherent disorder characterizing these resonances, no reliable trend could be identified for species B. A related method that employed the 2D MQ-MAS data presented in Figure 5a and b facilitated the extraction of two positive frequency points and two negative frequency points from these 8.45 and 14.1 T data. In this case, the apparent shift positions were supplemented by the 2D maxima (F_2 or MAS dimension) and vertical projections (F_1 or isotropic dimension), with the scaling of these shifts inducing an apparent sign change, thus positioning data points on both sides of the origin.[50] A graphical solution by this method (also given in Figure 4a) yielded a δ_{iso} value of −3.0 ppm and a P_Q value of 1.63 MHz for species B, the large difference between the δ_{iso} value of this and species C reflecting the very different degrees of water interaction for the Na tunnel window positions. Similar application of this method to species C provided data which were in good agreement with data obtained from the more conventional variable B_0 approach (see Table 1 and Figure 4a). The results of ^{23}Na 2D MQ-MAS analyses

(53) Koller, H.; Englehardt, G.; Kentgens, A. P.; Sauer, J. *J. Phys. Chem.* **1994**, *98*, 1544.
(54) Klosters, G.; Jansen, M. *Solid State Nucl. Magn. Reson.* **2000**, *16*, 279.
(55) Englehardt, G.; Sieger, P.; Felsche, J. *Anal. Chim. Acta* **1993**, *283*, 967.
(56) Felsche, J.; Luger, S.; Baerlocher, C. *Zeolites* **1986**, *6*, 367.
(57) Tijink, G. A. H.; Janssen, R.; Veeman, W. S. *J. Am. Chem. Soc.* **1987**, *109*, 7301.

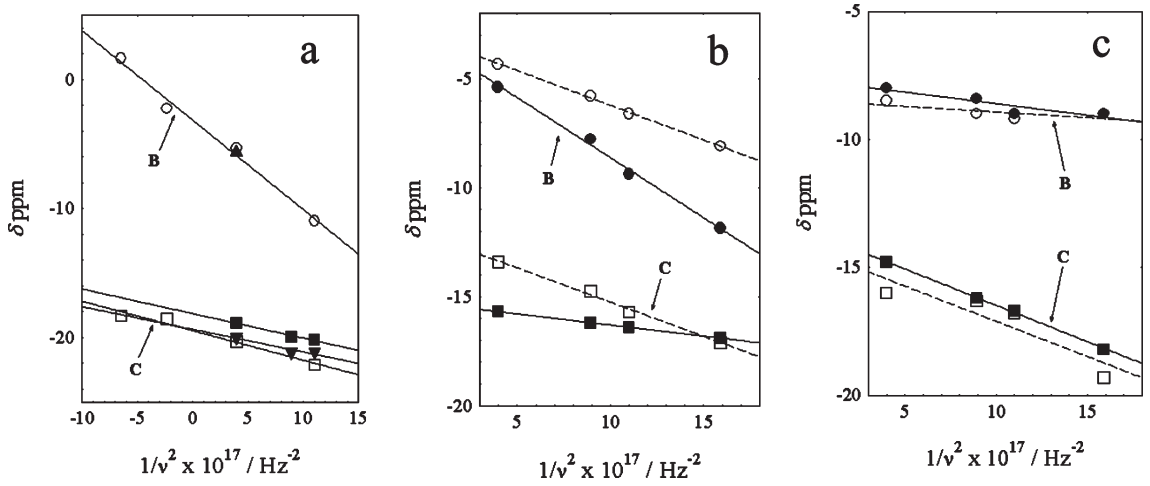

Figure 4. Field-dependent (B_0) ^{23}Na 1D MAS NMR data (solid symbols) and data derived from 2D MQMAS investigations (hollow symbols) for sodium species identified via simulation of spectra for (a) Na−W−HTB, (b) $Cs_{0.018}$− and $Cs_{0.154}$−W−HTB, and (c) $Sr_{0.019}$− and $Sr_{0.075}$−W−HTB.

Table 1. Refinement Parameters for the Simulation of ^{23}Na NMR Spectra of Na−W−HTB and Variably Exchanged Cs−W−HTB and Sr−W−HTB Phases

	species A NaO_6		species B $NaO_6(H_2O)_2$			species C $NaO_6(H_2O)$		
	δ_{iso} (ppm)	C_Q (MHz)	δ_{iso} (ppm)	P_Q (MHz)	$C_Q{}^a$ (MHz)	δ_{iso} (ppm)	P_Q (MHz)	C_Q (MHz)
$Cs_{0.018}$−W−HTB	−4.0	5.2	−3.1	1.49	2.98	−15.3	0.64	1.28
$Cs_{0.154}$−W−HTB	−4.0	5.2	−3.0	1.13	2.26	−12.1	1.12	2.24
$Sr_{0.019}$−W−HTB	−4.0	5.2	−8.5	0.42	0.84	−14.4	1.05	2.10
$Sr_{0.075}$−W−HTB	−4.0	5.2	−7.7	0.60	1.2	−13.6	1.07	2.14
Na−W−HTB	−4.0	5.2	nd	nd		−18.1	0.87	1.74
						−19.4	0.84	1.74
Na−W−HTB^b	na	na	−3.0	1.63	3.26	−19.3	1.05	2.10

^{a} $P_Q = C_Q\sqrt{(1+\eta^2/3)}$. ^{b} Using 2D MQ-MAS NMR data.

performed at 14.1 and 8.46 T for the Na−W−HTB phase are presented in Figure 5a and b.

The data acquired at both fields exhibited contours that clearly define species B and C and support the simulated data shown in Figure 2. Both data sets show that these contours are pitched at ~60−70° to the F_2 axis (or along the QCS or chemical shift distribution axis[42,58]), suggesting that the large degree of disorder exhibited by these species is dominated by chemical shift dispersion and not by a distribution in the quadrupolar parameters. This suggests that the positional disorder of both hydrated species B and C within the tunnel window site is minimal; however, there is probably a large distribution of Na−O(H_2O) bond lengths characterizing the coordination sphere of these mono- and dihydrated variants. From Figure 5a, it can be observed that the expected horizontal contour for species A (that exhibits characteristic short-range order) is not detected at 8.46 T due to the inefficiency of the RF pulses (B_1 = 110 kHz) in exciting to, and converting from, 3Q coherence pathways, with signal intensity being sacrificed as C_Q increases. The smaller C_Q/P_Q resonances thus dominate these 8.45 T data. However, in the 14.1 T MQ-MAS data of Figure 5b, very low intensity features describing a horizontal contour are just detectable above the baseline noise. These features are expected for a structural position exhibiting short-range order and minimal distributions affecting the chemical shift and quadrupolar parameters. These features were detectable for a number of reasons: the line shape at 14.1 T is narrower; these 2D data were acquired with stronger RF pulses (B_1 = 155 kHz); the 3Q conversion pulses implemented were enhanced by modulations; and the signal was detected as an echo. The latter helps to prevent broad signals such as those from species A from being lost in probe dead-times and beneath the resulting baseline distortions but requires an "echo" time period during which the ^{23}Na spins can lose coherence through T2 relaxation. This relaxation is the probable cause of the very different relative intensities observed for species B and C at 8.45 and 14.1 T. These descriptions of the tunnel Na speciation (species A, B, and C) for the Na−W−HTB phase are seemingly at odds with that elucidated from the diffraction studies. However, diffraction is not sensitive to the local chemical environment but rather sees the average structure which is being probed on a longer time scale relative to the NMR measurement. Thus, neutron and X-ray diffraction are simply inherently insensitive to the disorder and rapid exchange occurring in this system. This emphasizes the need for a multitechnique approach in order to develop accurate structure−function relationships for such adsorbent phases.

Additional ^{23}Na MAS NMR studies were undertaken on several Cs- and Sr-exchanged HTB systems to investigate the extent of the exchange process, and to ascertain whether the speciation of residual sodium occupying the tunnel window positions was altered upon extensive cation replacement. From the ^{23}Na MAS NMR data

(58) Angeli, F.; Charpentier, T.; Faucon, P.; Petit, J.-C. *J. Phys. Chem. B* **1999**, *103*, 10356.

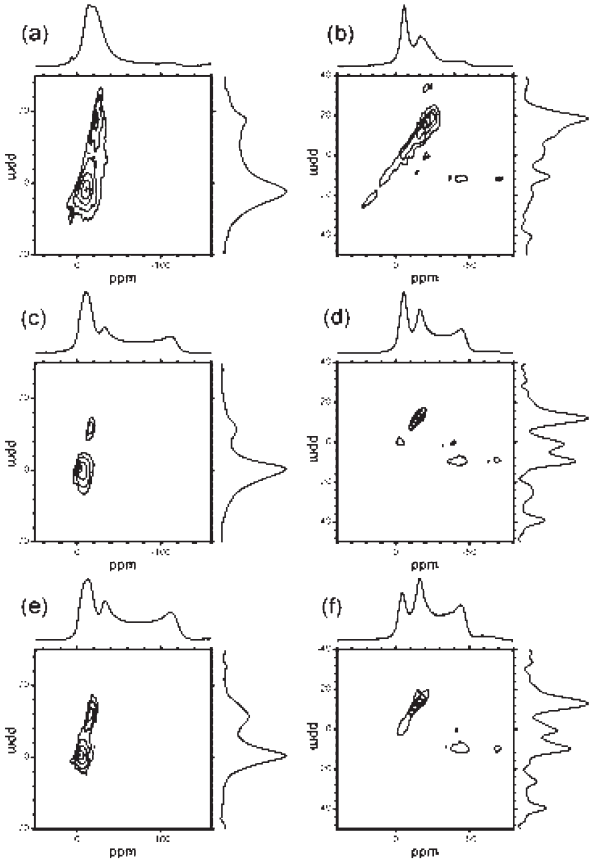

Figure 5. 2D ^{23}Na MQMAS NMR spectra for Na−W−HTB (a, b), $Cs_{0.018}$−HTB (c, d), and $Cs_{0.154}$−HTB (e, f) acquired at 8.45 and 14.1 T (left and right, respectively).

presented in Figures 6c,f for saturated Cs− and Sr−W−HTB samples, respectively, the presence of residual Na was unequivocal and easily detected, thus corroborating previous findings reported by Griffith et al.[33,34] and Reis et al.[29−32] In comparison to the spectrum of the parent Na−W−HTB (Figures 6c,f), the most obvious change to the Na tunnel speciation was the relative reduction of the hydrated species B and C resonances in comparison to the resonance of species A exhibiting the large quadrupolar interaction. As the level of Cs or Sr exchange increased, the population (total) of species B and C decreased in comparison to that of species A; that is, species B and C appear more exchangeable than species A. These data also indicate that this process is not identical for the Cs- and Sr-exchanged phases. The relative loss of the hydrated species B and C was far more pronounced after Sr exchange and is probably the consequence of the increased charge of this cation. In comparison, for the Cs−W−HTB phase, the ratio of species B to C was inverted, with the former appearing more favored. These observations appear driven by a lack of water available to hydrate the Na tunnel sites despite the water contents being comparable to the parent Na−W−HTB, that is, ∼5% w/w. We suggest that this is perhaps a result of a significant proportion of tunnel water being redistributed by these cations into larger occlusions by virtue of their much larger ionic (or hydrated) radii or because Cs^+ and Sr^{2+} cations each command their own extensive hydration spheres,

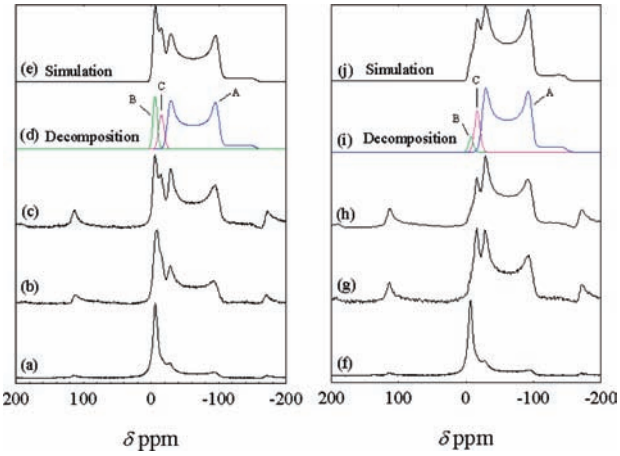

Figure 6. (a−j) ^{23}Na MAS NMR spectra acquired at 9.4 T of variably exchanged (left) Cs−W−HTB and (right) Sr−W−HTB. The spectrum of the parent Na−W−HTB at comparable B_0 is given in both.

which thus retard the transport of water through the tunnels.

It is important to note that the δ_{iso} (δ −4.0 ppm) and C_Q (5.2 MHz) parameters characterizing the resonance of species A are not significantly perturbed upon intermediate (Figure 6b,e) or high (saturation) (Figure 6c,f) Cs or Sr exchange, suggesting that the residual anhydrous Na^+ species (A) are sufficiently isolated from the exchanged Cs^+ and Sr^{2+} cations. This scenario differs considerably from what is reflected in the variable B_0 data of Figure 4b and c and Table 1 for species B and C, as these data clearly indicate that the introduction Cs^+ and Sr^{2+} cations (and the relative amounts) exerts a considerable influence on the δ_{iso} and P_Q (and hence C_Q) of the associated resonances. For the Sr−W−HTB system, an increasing degree of Sr exchange induced a downfield shift of δ_{iso} of ∼1 ppm for both species B and C, which were accompanied by minor increases in P_Q of ∼0.2 MHz and ∼0.02 MHz, respectively. Variations of this type and magnitude suggest that the hydrated Na^+ tunnel species are experiencing a marginally stronger (i.e., more ionic) interaction with the tunnel water, presumably caused by the more electropositive Sr^{2+} demanding a greater share of the available tunnel water to complete its hydration sphere. For the Cs−W−HTB system, more significant yet conflicting changes to the NMR parameters were measured: for species C, P_Q was observed to increase by ∼0.5 MHz and δ_{iso} underwent a large downfield shift of ∼3 ppm, while for species B, δ_{iso} was virtually unchanged and P_Q exhibited a decrease of ∼0.4 MHz, with increasing Cs exchange. Thus, substantially increasing ionic character appears to be characterizing species C presumably due to increased interaction with its coordinated water, resulting in smaller Na−O(H_2O) distances when Cs^+ is present.

A clear distinction that emerges upon Cs^+ or Sr^{2+} exchange in the HTB system is the marked reduction in line broadening observed for the ^{23}Na MAS spectra presented in Figure 6. The measured linewidths for species B and C in the parent material of ∼500−600 Hz reduced to ∼300−400 Hz in the Cs- and Sr-exchanged materials. A similar phenomenon was observed in the Cs−W−HTB 2D ^{23}Na MQ-MAS data (Figure 5c−f). The contours defining the presence of the hydrated Na

tunnel window species are more confined and exhibit greater definition, which is consistent with the reduced linewidths that characterize these systems. These contours maintain an orientation disposed along the QCS or chemical shift distribution axis, indicating that distributions of δ_{iso} values still influence the residual Na speciation; however, these distributions are now significantly diminished with respect to that observed for the parent Na−W−HTB phase. Such observations are consistent with a reduced influence of tunnel water on the residual Na speciation with each hydrated position experiencing less chemical exchange (from reduced water mobility) and a concomitant reduced distribution of Na−O bond lengths. In analogous fashion to the 2D ^{23}Na MQ MAS data for Na−W−HTB (Figure 5a and b), the excitation of the anhydrous Na site (species A) characterized by the large C_Q value has not been feasible. The 14.1 T data (Figure 5d and f) exhibit incomplete, low-intensity evidence of a horizontal contour expected for a short-range ordered site; however, a more complete measurement of this resonance would require extremely large RF power levels for efficient triple quantum excitation of the $(-3/2 \leftrightarrow +3/2)$ satellite transition.

3.3. Cesium and Strontium Ion Exchange Behavior — Radiochemical Investigations. In previous communications on the ion exchange behavior of the Na−W−HTB and molybdenum-doped variants (Mo−W−HTB), we presented the rapid kinetics and adsorption isotherms for the exchange of cesium and strontium from acidic media.[33,34] Briefly, the apparent selectivity of the Na−W−HTB phase in mildly acid solutions (1 M $[HNO_3]$) corresponds to the order Cs ≫ Ca > Sr > Na > K. Substitution of a small fraction of W by Mo affords increased selectivity for Sr under similar conditions so that the apparent order of selectivity then appears to be Cs ≫ Sr, Ca > Na > K (the effect of isomorphous substitution of molybdenum for tungsten in the Na−W−HTB phase will be discussed further in later sections). The radiochemical investigations conducted as part of this study using carrier-free ^{137}Cs (661 keV of ^{137m}Ba, 94.6%) and ^{85}Sr (514 keV, 99.3%) have confirmed the majority of these earlier results, which were determined using trace concentrations of Cs^+ and Sr^{2+} (ca. 0.1 mM).

It is well-known that, for an ideal, binary exchange process, there is a linear relationship for a plot of log K_d versus log $[H^+]$,[59] where the slope of this plot equals the negative of the charge ratio for the incoming cation (A^{Za}) and the exchangeable cations (B^{Zb}) of the given ion exchanger.[60,61] Employing this approach in the cesium and strontium exchange of the Na−W−HTB phase, the individual distribution coefficients for ^{137}Cs and ^{85}Sr were determined in nitric acid concentrations ranging from 0.5 to 9 M and the log of these values plotted versus log $[HNO_3]$ (Figure 7).[59]

These results showed a clear linear dependence for the exchange of ^{85}Sr with the slope being −1.806, demonstrating that the exchange of $2H^+$ within the

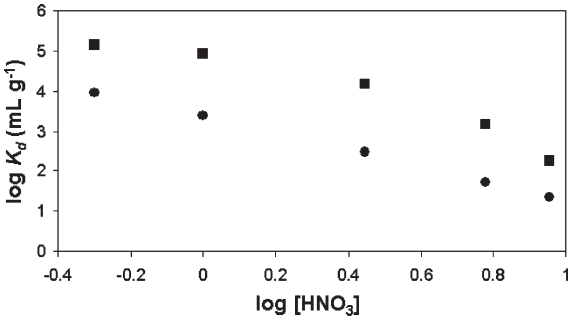

Figure 7. Plot of log K_d (distribution coefficient; mL g^{-1}) vs log $[HNO_3]$ for the adsorption of carrier-free ^{137}Cs (■) and ^{85}Sr (●) by Na−W−HTB. $V/m \cong 80$ mL g^{-1}.

HTB phase for Sr^{2+} is the dominant ion exchange reaction ($Sr^{2+} \leftrightarrow 2H^+$). In the case of ^{137}Cs, initial exchange appeared to conform to ideality (slope −1, $Cs^+ \leftrightarrow H^+$) at $[HNO_3] \leq 1$ M), but above this concentration the slope of the plot increased significantly to about −3.6 for 3, 6, and 9 M acid concentrations. Three possible reasons could explain the observed deviation from ideal behavior for the cesium exchange: (1) the selectivity coefficient, $K_{Cs/H}$, is sufficiently large even though C_B is still ≫ C_A which leads to a suppression of the log K_d versus log $[HNO_3]$[59] plot; (2) the $Cs^+ \leftrightarrow H^+$ exchange is not the dominant process controlling the observed ^{137}Cs K_d; (3) the site of cesium exchange is changing with increasing acid concentration. With respect to 1, the measured K_d values for ^{137}Cs adsorption at 0.5 and 1 M are exceptionally large, that is >80 000 mL g^{-1}, and are approaching the sensitivity limits of the radiochemical analysis under these counting conditions. Hence, it is possible that this could contribute significantly to the deviation of the log K_d versus log $[HNO_3]$ plot from linearity, but this then implies that the slope of the plot should only take into account the data points at higher acid concentrations where the slope is approximately −3. The second point highlights the reliance of the theoretical treatment on a binary ion exchange system, namely, $Cs^+ \leftrightarrow H^+$. In the case of the Na−W−HTB phase, both hydronium and sodium cations are present, and so there exists the potential for the $Na^+ \leftrightarrow {}^{137}Cs^+$ exchange to occur, especially since it has already been shown that the affinity of the Na−W−HTB phase for Cs^+ is much greater than that for Na^+ in mildly acidic solutions.[33,34] Although any small amount of Na^+ exchanged is unlikely to compete against the exchange of $^{137}Cs^+$ given the difference in selectivity, the same cannot be said with respect to $^{85}Sr^{2+}$. As the acid concentration is increased, the liberation of Na^+ from the HTB framework will potentially increase, and so the $H^+ \leftrightarrow Na^+$ exchange may become a significant factor.

Since the HTB materials have a unidimensional tunnel architecture, the presence of Na^+ within these tunnels has the potential to impede ion exchange. Difficulty in removing Na from silicotitanate ion exchangers has been noted and ascribed to tunnel crowding effects.[62] Given that the present materials have a fibrous morphology with a large aspect ratio (width of nanometers and length of micrometers), we hypothesize that it is difficult to achieve complete exchange of cations sited deep within the

(59) Decaillon, J. G.; Andres, Y.; Abbe, J. C.; Tournoux, M. *Solid State Ionics* **1998**, *112*, 143.
(60) Abe, M. In *Ion Exchange and Solvent Extraction*; Marcel Dekker: New York; Vol. *12*, Chapter 9, pp 381−441.
(61) Helfferich, F. *Ion Exchange*; McGraw-Hill Book Company: New York, **1962**.
(62) Poojary, D. M.; Bortun, A. I.; Bortun, L. N.; Clearfield, A. *Inorg. Chem.* **1996**, *35*, 6131.

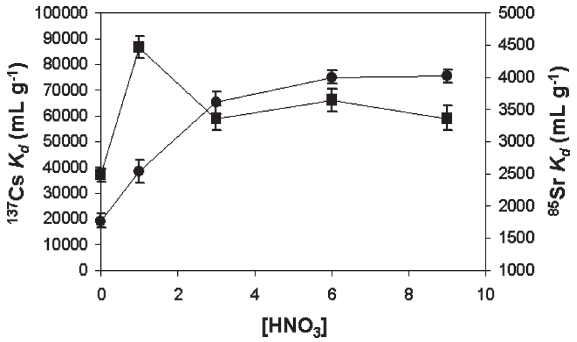

Figure 8. Plot of ^{137}Cs (■) and ^{85}Sr (●) K_d (distribution coefficient; mL g^{-1}) vs [HNO$_3$], which was used to pretreat the Na−W−HTB phase before use. $V/m \cong 80$ mL g^{-1}.

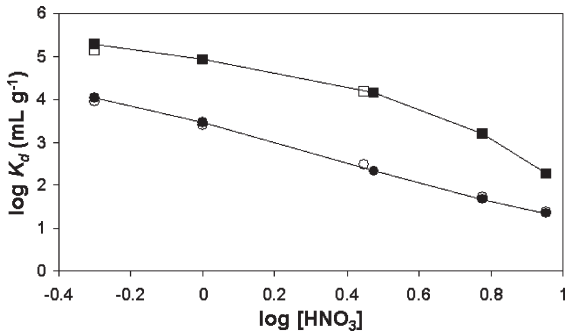

Figure 9. Plot of log K_d (distribution coefficient; mL g^{-1}) versus log [HNO$_3$] for the adsorption of carrier-free ^{137}Cs (■) and ^{85}Sr (●) by Na−W−HTB treated with concentrated HNO$_3$. The results of Figure 8 have been included for comparison as open symbols. $V/m \cong 80$ mL g^{-1}.

tunnels of these crystallites. Moreover, as the exchanging ion diffuses from both ends of the tunnels, Na^+ becomes trapped since the tunnels have diameters on the order of only 0.35 nm. Therefore, to further explore the contribution that the $Na^+ \leftrightarrow M^{x+}$ exchange has on the ion exchange behavior of the parent phase, the ^{137}Cs and ^{85}Sr distribution coefficients for Na−W−HTB phases, which had been pretreated with comparable acid strengths to that employed in the log K_d versus log [HNO$_3$] plot experiments, were determined and are presented in Figure 8. Since the samples of Na−W−HTB employed throughout this study were prepared using a washing step with 1 M HNO$_3$, the "0 M HNO$_3$" data points in Figure 8 were prepared by washing the as-prepared materials with deionized water only. In these samples, the level of initial $H^+ \leftrightarrow Na^+$ exchange should have been minimized. The Na−W−HTB phase treated with 1 M HNO$_3$ displayed increased K_d's for both ^{137}Cs and ^{85}Sr in mildly acidic solutions. The increase was most pronounced for ^{137}Cs, where the ^{137}Cs K_d increased to ~88 000 mL g^{-1} from ~38 000 mL g^{-1} for the 0 M HNO$_3$ phase. This increase was observed for several (five) different preparations of the "0 M" and "1 M" HNO$_3$ Na−W−HTB samples and translates to an increase in the percentage of ^{137}Cs extracted from 99.8% to 99.91%. Treatment of the Na−W−HTB phase with increasing acid concentration decreased the measured ^{137}Cs K_d to a consistent value of about 60 000 mL g^{-1}, as there was no statistical difference between the ^{137}Cs K_d's measured for the 3, 6, or 9 M acid concentrations.

The same general trend of increasing selectivity with increasing acid concentration was observed for ^{85}Sr uptake. However, in this case, the increase was far more progressive, and there was a statistically significant increase in K_d observed through to the 6 M HNO$_3$ data point. The ^{85}Sr K_d at this concentration was measured at ~4000 mL g^{-1}, which was almost a 3-fold increase from the 0 M HNO$_3$ data point, and corresponded to ~98% extraction of ^{85}Sr. These results suggest that there is a definite advantage in ensuring that any easily exchanged Na^+ is removed from the HTB phase prior to exchange with strontium. Therefore, where the adsorption of a cation, for which the W−HTB lattice exhibits a lower affinity than that of Sr^{2+}, for example, Co^{2+}, is concerned, the presence of residual sodium (and other competing ions) will drastically affect the observed level of adsorption and reproducibility.

Nonetheless, the ideality observed in Figure 7 for ^{85}Sr adsorption demonstrates that exchange in even 1 M HNO$_3$ must be able to ensure that there is a sufficient concentration of hydronium ions within the W−HTB lattice, such that ion exchange predominately occurs via a $Sr^{2+} \leftrightarrow 2H^+$ exchange process. Given that the ^{137}Cs K_d and, hence, selectivity were not dramatically affected by Na^+ present either within the W−HTB lattice or in solution as a competing cation, this seemingly suggests that the nonideality of the ^{137}Cs exchange is due to a change to the W−HTB lattice, structural or otherwise. This conclusion is supported by the results presented in Figure 9, where Na−W−HTB, which had been treated to remove as much sodium as possible using 9 M HNO$_3$, still exhibited ideal exchange of ^{85}Sr and nonideal exchange of ^{137}Cs.

To explore whether any structural change to the W−HTB framework resulted from contact with increasing acid concentrations, X-ray diffraction patterns of the Na−W−HTB phases treated with 0−9 M HNO$_3$ were acquired and refined using Rietveld techniques. The X-ray diffraction patterns were refined using the parameters derived from the previous neutron diffraction studies as a starting point. Due to the insensitivity of X-rays to the presence of either hydroxide or water molecules, this led us to remove this possibility from the associated refinements. The occupancies of the sodium position and water molecules within the framework tunnels were fixed using results from the XRF and TG/DT analyses of the respective Na−W−HTB phases, as the initial refinement of each parameter yielded occupancies which were highly improbable. In Figure 10 are shown the individual unit cell volumes plotted along with the respective ^{137}Cs and ^{85}Sr K_d values. Selected crystallographic parameters are given in Table 2. The most striking feature that arose from these structural analyses was the decrease in the unit cell volume of the "0 M HNO$_3$" phase from 180.8 Å^3 to 180.3 Å^3 for the Na−W−HTB phase pretreated with 1 M HNO$_3$. Treatment with increasing acid concentrations resulted in ostensibly little change to the unit cell volume, even when the phase was contacted with concentrated HNO$_3$. If nothing else, this type of pretreatment with concentrated acid demonstrates the stability that the W−HTB lattice has under acidic conditions. The results of the XRF analysis and the measured sodium stoichiometry (Na/W ratio) for the respective acid treatments are also

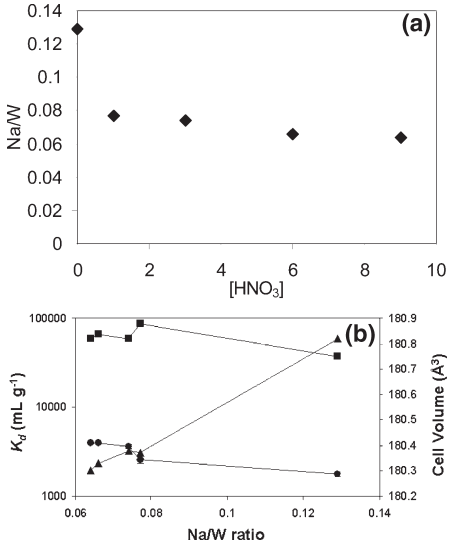

Figure 10. (a) Plot of Na/W ratio determined by XRF as a function of the acid concentration used for pretreatment and (b) ^{137}Cs (■) and ^{85}Sr (●) K_d (distribution coefficient; mL g^{-1}) and refined unit cell volume (Å^3, ▲) vs Na/W ratio for Na−W−HTB treated with varying [HNO_3].

Table 2. Crystallographic Parameters for Na−W−HTB Phases Treated with Increasing Concentrations of Nitric Acid

	R_p	R_{wp}	cell (Å^3)	a (Å)	c (Å)	Na
0 M	2.93	4.94	180.828(6)	7.327(2)	3.889(1)	0.17(8)
1 M	2.97	4.94	180.354(4)	7.320(6)	3.886(0)	0.13(9)
3 M	2.94	4.88	180.377(0)	7.322(1)	3.884(8)	0.13(3)
6 M	2.92	4.81	180.334(6)	7.321(8)	3.884(3)	0.13(1)
9 M	3.24	6.21	180.307(3)	7.322(0)	3.883(5)	0.12(5)

presented in Figure 10. The plots clearly demonstrate that treatment with only 1 M HNO_3 is sufficient to remove almost 40% of the sodium present in the as-prepared Na−W−HTB phase. Although the sodium stoichiometry continued to decrease with increasing acid concentration, the change was relatively minor with respect to this initial decrease. These results strongly suggest a correlation between the sodium stoichiometry and unit cell volume of the HTB phase. This is perhaps not surprising given the degree of flexibility that we have observed during the low-temperature thermal studies of Na−W−HTB and Cs-exchanged W−HTB phases, that are reported in a companion article in this journal.[63] As the simultaneous TG−DT analysis of the phases containing variable sodium showed that the relative hydration levels are comparable, that is, ∼5% w/w, we believe that the change in unit cell volume is predominately a result of the level of sodium present within the framework and not purely water content.

In light of the structural and compositional analysis of the acid-treated Na−W−HTB phases, it appears that the ^{137}Cs and ^{85}Sr distribution coefficients of these materials are influenced to varying extents by these two aspects. Given our previous observation of the minimal competitive cation effect of sodium on cesium adsorption, we hypothesize that changes in the unit cell volume of the Na−W−HTB phase is the predominant factor contributing to the observed ^{137}Cs distribution coefficients for the various acid-treated materials and indeed the overall

(63) Luca V.; Griffith, C. S.; Hanna, J. V. *Inorg. Chem.* **2009**, *48*, DOI: 10.1021/ic801295c.

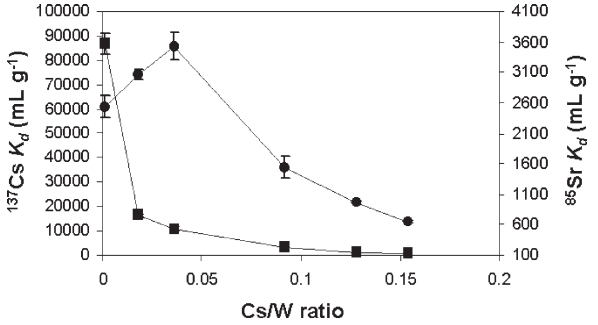

Figure 11. Plot of ^{137}Cs (■) and ^{85}Sr (●) K_d (distribution coefficient; mL g^{-1}) vs cesium-exchange level in Cs−W−HTB. $V/m \cong 80$ mL g^{-1}.

selectivity. Although similar considerations must be given to interpretation of the ^{85}Sr adsorption studies, the observed ^{85}Sr K_d continued to increase significantly (statistically) with decreasing sodium content, while the unit cell volumes of the W−HTB phases remained relatively constant. Hence, we surmise that the decreasing level of sodium present in the HTB phases is principally responsible for the progressive increase in the ^{85}Sr distribution coefficient. Precisely whether this effect is due to the increased number of ion exchange sites with hydronium ions (rather than Na^+), an increased ability of Sr^{2+} to diffuse through the HTB framework, or a decrease in liberated Na^+ acting as a competing cation against $^{85}Sr^{2+}$ is unclear.

The results of the neutron diffraction and particularly the ^{23}Na solid-state NMR studies of the A−W−HTB (A = Na, Cs and Sr) phases showed that, although there appears to be varying degrees of positional disorder and interaction with coordinated water for sodium, cesium, and strontium within the tunnels of the W−HTB lattice, each of the cations reside at, or near, the center of the hexagonal window of the tunnel framework. On this basis, there is little structural evidence that suggests that two distinctive ion exchange sites exist within the HTB framework. However, the question of unique ion exchange sites for cesium and strontium was probed further by determining the individual ^{137}Cs and ^{85}Sr K_d's for Na−W−HTB exchanged with macromolar levels of inactive cesium or strontium. The exchange of cesium and strontium was undertaken in 1 M HNO_3 and the materials isolated, dried, and stored in an analogous manner to that of the parent Na−W−HTB. The maximum degree of cesium and strontium exchange represents approximately 80% of the theoretical cation exchange capacity (CEC) for each of the individual cations and the Na−W−HTB phase.[33,34] The ^{137}Cs and ^{85}Sr distribution coefficients of variably exchanged Cs−W−HTB and Sr−W−HTB phases were then determined individually in 1 M HNO_3, and the results are presented in Figures 11 and 12, respectively. These results clearly show that, even with low levels of exchanged cesium or strontium, the distribution coefficient for the corresponding radiotracer was significantly less than that of the parent Na−W−HTB. In the case of Cs−W−HTB, the ^{137}Cs K_d decreased from 88 000 mL g^{-1} to 18 000 mL g^{-1} upon exchange of only 0.02 mmol g^{-1} (10% of the CEC) of inactive cesium. With respect to Sr−W−HTB, the ^{85}Sr K_d decreased from 2544 mL g^{-1} to 254 mL g^{-1} upon exchange of only 0.019 mmol g^{-1}

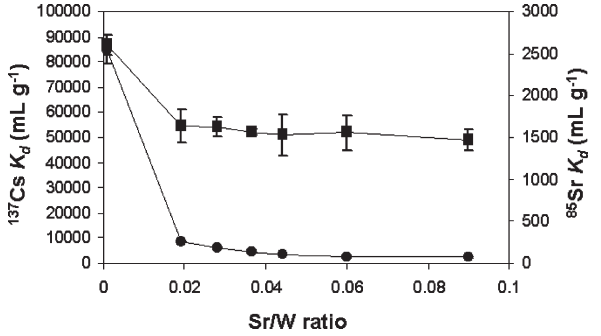

Figure 12. Plot of ^{137}Cs (■) and ^{85}Sr (●) K_d (distribution coefficient; mL g^{-1}) vs strontium-exchange level of Sr−W−HTB in 1 M HNO_3. $V/m \cong 80$ mL g^{-1}.

(16% of the CEC) of inactive strontium. At the maximum level of cesium and strontium exchange for the Cs−W−HTB and Sr−W−HTB phases, the ^{137}Cs and ^{85}Sr K_d's decreased further to 613 and 75 mL g^{-1}, respectively.

In comparison, the data from the exchange of ^{85}Sr for the variably exchanged Cs−W−HTB phases showed significantly different behavior. Exchange of up to 0.036 mmol g^{-1} (~18% of the CEC) of cesium in fact resulted in a statistically significant increase in the ^{85}Sr distribution coefficient. With higher levels of cesium exchange, the ^{85}Sr distribution coefficient progressively decreased to 651 mL g^{-1} at the maximum level of exchange. For the exchange of ^{137}Cs with variably exchanged Sr−W−HTB, even at the lowest level of strontium exchange, a decrease of the ^{137}Cs distribution coefficient to 55 000 mL g^{-1} was observed, but as the level of strontium exchange increased, statistically the ^{137}Cs distribution remained unaltered.

The power of employing radioanalytical methods to study ion exchange reactions lies first in the analytical efficiency of such an approach but also because the extremely low concentrations of the radioisotope involved means that the site of exchange for one cation is likely to be significantly removed from that of another cation exchange, assuming that there is a significant excess of ion exchange sites. Such a scenario means that the subtle features of the individual ion exchange reactions can be probed without interference arising from exchange at adjacent sites, that is, saturation effects. If one first considers the results from the increasing macromolar levels of cesium and strontium exchange, it is not surprising that the distribution coefficients for ^{137}Cs and ^{85}Sr, respectively, concomitantly decrease as the sites for ^{137}Cs and ^{85}Sr exchange become less prolific. Increased levels of exchange increase the likelihood of an empty ion exchange site being close to, or adjacent to, an already occupied (with an inactive cation) ion exchange site. Moreover, the degree of repulsion between incoming ^{137}Cs and ^{85}Sr cations and cations already exchanged within the tunnels would also be expected to increase and suppress the observed distribution coefficient. This effect has been referred to by several researchers as the "field gradient" of a given ion exchange phase and is often responsible for the selectivity reversal of an ion exchanger as its capacity for a given cation is approached.[59] Similar factors are also applicable if one considers that only a single type of ion exchange site is present and the exchange of a cation which is now different from that which already resides at the ion exchange site occurs. However, in the case where two unique ion exchange sites are present, with their own unique selectivity for given cations, a degree of "insulation" of the selectivity of the ion exchange phase for the incoming cation, from the level of a different cation already residing in the ion exchanger, would be expected. This scenario appears akin to the results obtained for the exchange of ^{85}Sr and ^{137}Cs by the variably exchanged Cs−W−HTB and Sr−W−HTB phases, respectively. With the existence of potentially unique ion exchange sites, the eventual decrease in the ^{85}Sr distribution coefficient at cesium exchange greater than 0.036 mmol g^{-1} could be rationalized by the expectation of increasing difficulty of a divalent cation to diffuse to the available ion exchange sites of the Cs−W−HTB phase as the level of cesium also increases. The selectivity of the variably exchanged Sr−W−HTB phases for ^{137}Cs certainly demonstrates that the level of macromolar strontium does not appear to dictate the ^{137}Cs selectivity to any large degree. However, does this necessarily support the possibility of two unique ion exchange sites for cesium and strontium? First, consider that the maximum strontium exchange of 0.08 mmol g^{-1} is still less than the calculated theoretical exchange capacity for strontium of 0.12 mmol g^{-1}. Although this appears quite close to the theoretical capacity, in terms of a monovalent cation (such as $^{137}Cs^+$), this actually equates to 0.08 mmol g^{-1} of remaining capacity, or approximately 4×10^{-6} remaining ion exchange sites per contact experiment. Given that the amount of ^{137}Cs radiotracer employed in each experiment is on the order of picomoles, it would appear that only at the upper levels of strontium exchange might the ^{137}Cs selectivity be drastically impacted by saturation effects. The increase of ^{85}Sr K_d's at low levels of Cs exchange is then most probably an artifact of the initial cesium exchange where any easily exchangeable sodium from the W−HTB framework is removed (by H_3O^+ or Cs^+ exchange), thereby limiting competitive cation effects during the adsorption of ^{85}Sr.

3.4. Molybdenum Doping of the HTB Framework. As we have reported previously,[33] a proportion of the tungsten in the W−HTB framework can be substituted for molybdenum through the incorporation of sodium molybdate during hydrothermal synthesis. These phases are poorly crystalline as judged from their X-ray diffraction patterns. Moreover, the progressive loss of the [001] reflection with an increasing atom percent content of molybdenum indicated that the HTB lattice contained significant disorder in the $a-b$ plane. It should be noted again that the difficulty in extracting meaningful structural data from these materials using scattering techniques was the reason we focused on the parent Na−W−HTB phase in this study. We also reported that substitution of about 3% of molybdenum for tungsten was the optimum level, which resulted in an increase in selectivity for Sr (in 1.0 M HNO_3), and that the apparent order of selectivity for the HTB phase corresponded to Cs ≫ Sr, Ca > Na > K. Given the subtle differences observed for ^{137}Cs and ^{85}Sr selectivity, w.r.t. cation loading, and so forth in the investigations outlined above,

we decided to revisit a series of Mo-doped HTB phases (0−20% Mo content) using radioanalytical techniques.

The series of molybdenum-doped HTB phases investigated (Mo_y−W−HTB, y = doping level atom %) was prepared using the previously outlined synthetic procedure at y = 0, 5, 10, and 20. The compositional analyses of the molybdenum-doped phases by STEM-EDS revealed molybdenum atom percentages of 7, 13, and 24 atom % for the three phases, namely, $Na_{\sim 0.13}Mo_{0.07}W_{0.93}O_3 \cdot zH_2O$, $Na_{\sim 0.06}Mo_{0.13}W_{0.87}O_3 \cdot zH_2O$, and $Na_{\sim 0.05}Mo_{0.24}W_{0.76}O_3 \cdot zH_2O$ and, as such, were marginally higher than the target levels.

The XRD patterns of these four phases are shown in Figure 13 and are consistent with those reported previously. Analysis of the parent Na−W−HTB phase (y = 0) by STEM revealed that the phase consisted of well-formed, rod-shaped crystallites (Figure 14a and b). The aspect ratio of the observed crystallites was about 10 (length/width), with the largest particles observed being about 1 μm in length (Figure 14a). Compositional analysis of a range of particle sizes by EDS revealed no observable differences between the crystallites and compositions which were consistent with that reported for material treated in accord with the method outlined in the Experimental Section. Micrographs from the STEM examination of the Mo_y−W−HTB (y = 7, 13, and 24) phases are shown in Figure 14c and d, e and f, and g and h, respectively. These results appear to indicate a progressive shift from well-formed, rod-shaped crystallites (parent Na−W−HTB phase) to thin fibrils (Mo_{20}−W−HTB) as the level of molybdenum incorporation was increased. Furthermore, "clumping" of smaller crystallites appeared more prominent as molybdenum incorporation was increased.

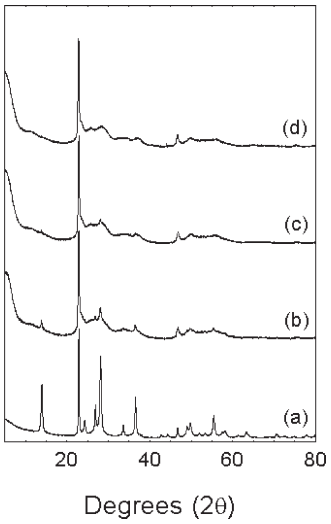

Figure 13. Powder X-ray diffraction patterns of Mo_x−W−HTB with (a) x = 0, (b) x = 5, (c) x = 10, and (d) x = 20 atom %.

Given that the preparation of specimens on holey carbon grids for STEM analysis is prone to sampling inconsistencies, we also attempted to determine the bulk particle size characteristics of each phase using laser diffraction. The determined particle size distributions for the y = 0−24 samples are presented in Figure 15. The plots demonstrate that as Mo atom percentage was increased from 0 to 24 atom %, the mean particle size for the bulk materials progressively decreased from 10.3 to 4.33 μm. This physical trait should be considered further when assessing the ion exchange properties (see later). What was also apparent was the range and bimodal nature of the y = 0 and 7 materials' particle size distributions. Both of these materials appeared to contain smaller particles of about 0.12 μm size, and from analysis of the distribution plots for various preanalysis runs, we believe that this smaller size fraction is due to the degree of ultrasonics required to successfully disperse these samples. The range of particle sizes present in the y = 0 sample was also reflected in the analysis of the particle size data (Table 3) where both the D_v90 and D_v50 values for the y = 7 sample were about half that of the former. However, this trend does not continue with the y = 13 and 24 sample's D_v90 or D_v50 values, as the presence of the 0.12 μm fraction tends to skew the values toward smaller particle sizes. Regardless, the particle size determinations clearly demonstrated that, for the "bulk samples", increased molybdenum-doping leads to a steady decrease in the average particle size, which is in accord with the general trend observed by STEM.

Extensive examination of the Mo_y−W−HTB (y = 5, 10, and 20) phases (and a duplicate series) by STEM-EDS confirmed the level of molybdenum incorporation and demonstrated that all samples were monophasic. First, with increasing molybdenum content, the level of sodium concomitantly decreased, to the point where, for the Mo_{20}−W−HTB phase, the level of sodium was close

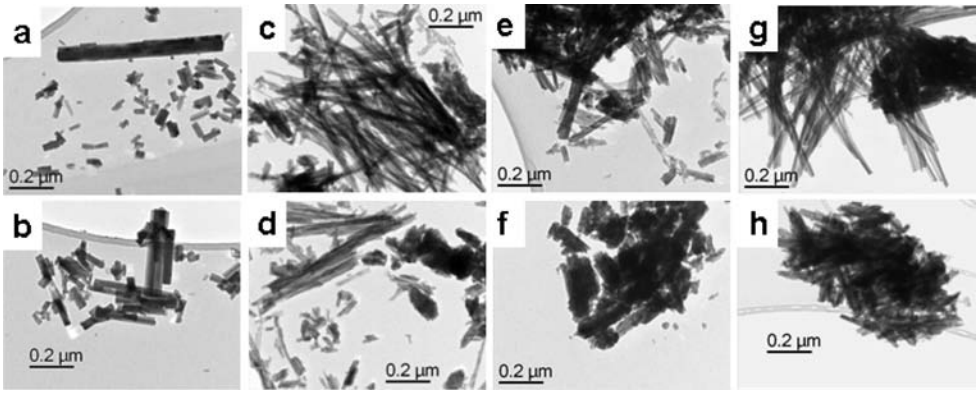

Figure 14. STEM micrographs of (a and b) $Na_{0.14}WO_3 \cdot zH_2O$, (c and d) $Na_{\sim 0.13}Mo_{0.07}W_{0.93}O_3 \cdot zH_2O$, (e and f) $Na_{\sim 0.06}Mo_{0.13}W_{0.87}O_3 \cdot zH_2O$, and (g and h) $Na_{\sim 0.05}Mo_{0.24}W_{0.76}O_3 \cdot zH_2O$.

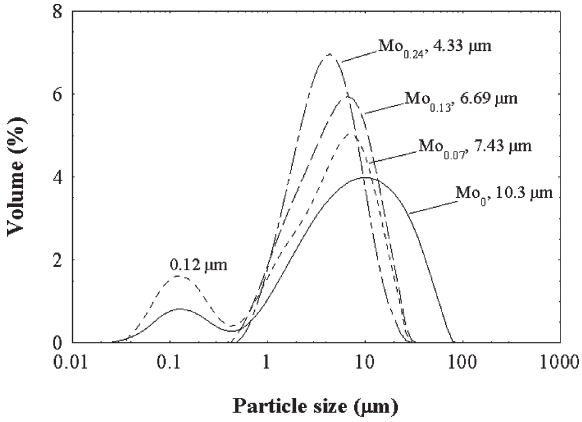

Figure 15. Volume percentage versus particle size (μm) plots for Mo_x−W−HTB (x = 0, 5, 10, and 20 atom %) phases.

Table 3. Particle Size (μm) Data for Bulk Mo_y−W−HTB (y = 0, 5, 10, and 20 atom %) Phases Determined Using Laser Diffraction[a]

Mo atom%	D_v10	D_v50	D_v90
0	0.596	7.432	32.873
7	0.153	4.182	13.842
13	1.457	5.346	14.842
24	1.525	4.247	10.787

[a] D_v10 = 10% < x; D_v = 50% < x; D_v90 = 90% < x.

to the practical detection limit (~$Na_{0.05}$) of the EDS analysis. This could be due to the decreasing particle size (about 10 → 4 μm) allowing more ready exchange of sodium, but we believe that the increasing disorder of the lattice with increasing molybdenum is the most likely reason. The levels of molybdenum-doping indicated by the EDS analyses were surprising given our previous investigations, which indicated that the solid-solution limit for molybdenum in the HTB phase was only about 3−5 atom %. Reanalysis of the materials employed for our first study has revealed compositions consistent with those found for the materials synthesized as part of this study, and we suggest that the initial analyses may have been affected by incorrect calibration of the EDS system. However, the precise reason remains unclear. Nonetheless, the selectivity of the variably molybdenum-doped phases (duplicates) for ^{137}Cs and ^{85}Sr from 1.0 M HNO_3 were investigated, and the associated distribution coefficients are presented in Figure 16. In the case of the ^{137}Cs distribution coefficients, the observed behavior was very different from that of ^{85}Sr with the ^{137}Cs K_d decreasing dramatically on incorporation of molybdenum. The observed ^{137}Cs K_d decreased from 90 000 mL g^{-1} for the parent Na−W−HTB phase to 45 000 mL g^{-1} for the Mo_5−W−HTB phase, then down to 25 000 mL g^{-1} for the Mo_{20}−W−HTB phase. Increased molybdenum doping of the W−HTB framework had a positive effect on the selectivity for strontium, with the K_d increasing from 2500 mL g^{-1} for the parent Na−W−HTB to 6500 mL g^{-1} for the Mo10−W−HTB phase. Statistically, there is no difference between the ^{85}Sr K_d for the Mo_{10}−W−HTB and Mo_{20}−W−HTB phases. Importantly, both of the trends in selectivity and individual reproducibility were reconfirmed for ^{137}Cs and ^{85}Sr adsorption with a duplicate series of Mo_y−W−HTB (y = 0−20) phases.

In our initial report on molybdenum incorporation, similar behavior to that presented here for strontium was

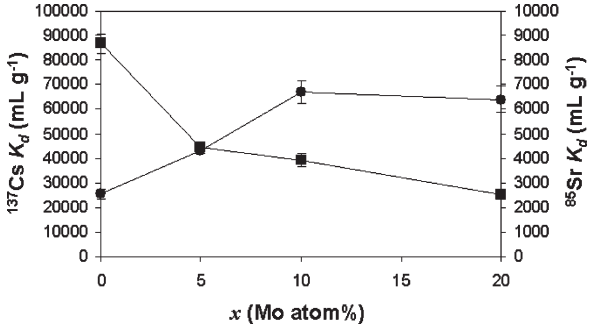

Figure 16. Plot of ^{137}Cs (■) and ^{85}Sr (●) K_d (distribution coefficient; mL g^{-1}) versus x (Mo atom %) in 1 M HNO_3. $V/m \cong 80$ mL g^{-1}.

observed; namely, about 10 atom % Mo was the optimum substitution level for molybdenum. However, the radioanalytical investigations of this study demonstrate that any incorporation of molybdenum into the HTB framework has a deleterious effect on its selectivity for cesium. We believe this behavior is intimately linked to the increasing disorder of the W−HTB framework with increasing molybdenum content, as this would also disrupt the structure of the tunnel ion exchange sites. Indeed, it is our hypothesis that this applies for all cations which are strongly bound by the W−HTB framework. Where the W−HTB framework exhibits lower affinity for a cation, such as Sr^{2+}, the presence of competitive cations such as sodium has the potential to dominate the ion exchange behavior. In the case of molybdenum doping, we believe that this is the reason for the increase in affinity with increasing molybdenum, given the decreased level of sodium in these samples. Hence, we find a recent report[64] purporting that molybdenum doping of the W−HTB framework does not result in a systematic change to the selectivity, quite puzzling in light of the investigations reported here and numerous other studies by our group. We suspect that the influence of the (not so) subtle effects of competitive cation concentration, adsorbed cation speciation, and ion exchange site structural aspects have been neglected by these researchers.

4. Conclusions

The structural investigations of the hexagonal tungsten bronze framework using neutron scattering, X-ray diffraction, and MAS NMR studies all point to the tunnel cations residing at the middle of the hexagonal tunnel windows formed by the corner-sharing W octahedra, as found initially by Reis and co-workers. This study has unequivocally shown that the selectivity of the W−HTB framework for cesium is defined by the structure of the hexagonal window, ion exchange site. Compromising the geometry of this window even in the slightest way by either (1) varying the cell volume through changes to hydration or sodium content or (2) introducing disorder in the a−b plane through molybdenum doping is sufficient to reduce the selectivity.

The structural investigations and interpretations thereof also indicate that strontium resides at a similar position to cesium but that the positional disorder and mobility of species within the tunnels are higher than in the case of cesium. This study has unequivocally shown that the affi-

(64) Smith, S. V.; Fuchs, A.; Kennedy, S. *J. Labelled Comps. Radiopharm.* **2005**, *48*, S12–S18.

nity of the W−HTB framework for Sr^{2+} is less than that of Cs^{+} and is most probably due to the slightly smaller effective size of Sr^{2+}; namely, it is less of a good fit for the hexagonal window, ion exchange site. The effect of competing cations (Na^{+}, K^{+}, and Ca^{2+}) is far greater in the case of Sr^{2+}, and this is a particularly important aspect to appreciate since there is always Na^{+} present in the Na−W−HTB phase. As such, any interpretation must be conducted as a ternary exchange system, namely, a H^{+}/Na^{+} solid−M^{x+} solution. The strong link between the residual sodium content of the Na−W−HTB or Mo_y−W−HTB phases and the observed ^{85}Sr K_d leads us to propose that this is the principal factor defining the affinity of the phases. Clearly, the influence of competing cations is crucial to the adsorption of cations for which the W−HTB lattices display even less affinity.

It is poignant to note that direct comparison of our previous observations of cesium and strontium selectivity for variably molybdenum-doped W−HTB phases and the radiotracer results reported here are somewhat difficult given the milligram per liter concentrations employed for our initial studies. However, it is highly likely that, for the adsorption of macro quantities of cesium and strontium, our initial results were influenced by both "selectivity" and "capacity". In the current radiotracer study, we are certainly not observing any influence due to "capacity", given the nanomolar quantities employed.

Supporting Information Available: Neutron diffraction refinement plots are available, in addition to crystallographic parameter tables. This material is available free of charge via the Internet at http://pubs.acs.org.